

Extracting the tropospheric short-wave influences on subseasonal prediction of precipitation in the United States using CFSv2

Martin Schroeder^{1,2} · S.-Y. Simon Wang^{1,2} · Robert R. Gillies^{1,2} · Huang-Hsiung Hsu³

Received: 3 February 2016 / Accepted: 8 August 2016 / Published online: 24 August 2016
© Springer-Verlag Berlin Heidelberg 2016

Abstract The development of subseasonal precipitation forecasts on regional scales is becoming an active area of research. Climate forecast models have shown deficiencies in predicting the extreme precipitation anomalies at medium to long-range timescales. This study explores the subseasonal relationships between tropospheric short-waves and regional precipitation anomalies across the continental United States and evaluates capabilities of the NCEP Climate Forecast System Version 2 (CFSv2) in resolving these relationships. A regional precipitation proxy is derived from the prediction of the upper tropospheric short-waves based on multiple linear regressions. Across the six climate regions defined by NOAA, the 30-day reforecasts of this short-wave based precipitation proxy are compared to identify the combinations of month and zonal wavenumber that exhibit the highest prediction score. Forecast of this precipitation proxy over certain regions is found to outperform the direct precipitation output of CFSv2 out to 4 weeks, suggesting a subseasonal predictability in precipitation that can be harvested from persistent circulation features.

Keywords CFSv2 · Shortwave teleconnections · Subseasonal precipitation forecasting · Midlatitude dynamics

1 Introduction

There is now substantial evidence that extreme wet/dry climate anomalies at the regional scale are frequently associated with a meandering, quasi-stationary jet stream that directs Rossby wave energy fluxes of a particular configuration; this mechanism is referred to as the circumglobal teleconnectivity (CGT) (Ambrizzi et al. 1995; Branstator 2002; Ding and Wang 2005). In North America, it has been found that amplified, mid-latitude, short-wave patterns often accompany wet/dry extremes. For instance, Screen and Simmonds (2014) estimated that significantly amplified circulation anomalies within zonal wavenumbers 3–8 were present in 40 % of the months that featured extreme precipitation episodes. While extreme conditions are often tied to a range of wavenumbers, pronounced CGT dynamics frequently present with a zonal wavenumber 5 (wave-5) structure (Branstator 2002; Ding and Wang 2005; Wang et al. 2010; 2013a). Moreover, previous studies have identified CGT patterns affecting both winter time (Hoskins and Ambrizzi 1993; Ambrizzi et al. 1995; Branstator 2002) and summer time (Ding et al. 2011; Wang et al. 2010, 2013a; Schubert et al. 2011) precipitation patterns across North America. For this study, we specifically target the CGT pattern with a focus on the zonal wavenumbers 4, 5 and 6, referred to as *short-wave* patterns throughout this manuscript.

While various studies have identified stationary CGT patterns as an important driver of subseasonal climate variability and extremes (Schubert et al. 2011, Wang et al. 2013a, 2014), achieving skillful climate prediction of extreme events remains a challenge. In general, medium to long-range numerical weather prediction models have difficulty in forecasting the location and intensity of prolonged precipitation anomalies. A number of studies (Yuan et al. 2011; Sooraj et al. 2012; Saha et al. 2014) have evaluated

✉ Martin Schroeder
martin.schroeder@aggiemail.usu.edu

¹ Utah Climate Center, Utah State University, Logan, UT, USA

² Department of Plants, Soils, and Climate, Utah State University, Logan, UT, USA

³ Research Center for Environmental Changes, Academia Sinica, Taipei, Taiwan

the skill in precipitation forecasts by the NCEP Climate Forecast System Version 2 (CFSv2) model, concluding that over the full reforecast period (1982–2010) virtually zero skill exists past the 2-week range. Becker et al. (2013) narrowed the scope of the CFSv2 prediction analysis to focus on “short-term climate”, which included monthly means at extended lead times, and found an increase in the skill metrics when considering only extreme precipitation forecasts across North America. However, Becker et al. (2013) argued that even with the increase in skill metrics, overall skill in precipitation forecasts of monthly means remains negligible.

To date, the potential skill of CFSv2 in predicting the aforementioned linkage between upper-level circulation anomalies associated with the CGT pattern and resultant precipitation anomalies has not been examined. Previous studies tying the large-scale circulations to forecasting persistent surface weather events, such as the wintertime valley temperature inversions in Utah (Gillies et al. 2010) and summer afternoon thunderstorm episodes on a subtropical island (Wang et al. 2013b), have shown that CFSv2 retains a longer prediction window for up to 4 weeks. It is with this in mind that the research undertaken and analysis reported here considered: (a) CFSv2’s ability to resolve the linkage between synoptic-scale planetary waves (i.e. short-waves) and corresponding regional precipitation anomalies with extended lead times and, (b) applicability of (a) towards the improvement of subseasonal forecasts of precipitation for different regions and in different times of the year.

2 Data sources

Given this study’s focus on the predictive capabilities towards short-wave circulations and regional precipitation, we utilized the fields of geopotential height (Z) and precipitation (P) from the following datasets: (a) the NCEP Climate Forecast System Reforecast (CFSv2) (Saha et al. 2014), (b) the National Centers for Environmental Prediction/National Center for Atmospheric Research Global Reanalysis (NCEP1) dataset (Kalnay et al. 1996), and (c) daily station-derived gridded precipitation from the Climate Prediction Center rain gauge analysis (a.k.a. U.S. Mexico Precipitation Analysis) (Chen et al. 2008). Using these datasets, we created a running 30-day series of 200 hPa Z and normalized P from both observations and reforecasts over the period 1982–2009. All variables were re-gridded onto a $2.5^\circ \times 2.5^\circ$ resolution grid for comparison with the NCEP1 dataset. The CFSv2 200 hPa (Z_{CFS}) and precipitation rate (P_{CFS}) fields were available every 5 days and so, 30-day averages representative of each month were computed using the initialization date nearest

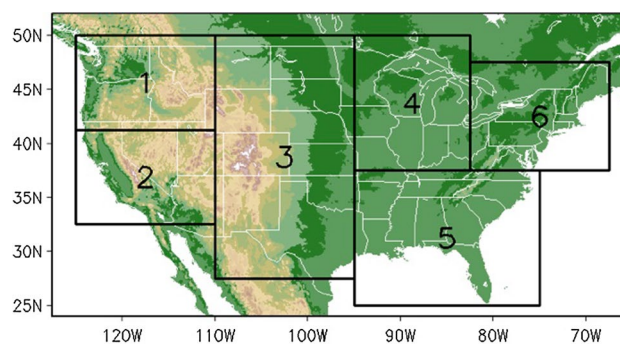


Fig. 1 Six study regions (R1–R6) for the conterminous United States. Taken from National Climate Assessment (NCA) and plotted on a $2.5^\circ \times 2.5^\circ$ grid. (http://www.epa.gov/global-adaptation/iclus/nca_regions.html)

to the start of the month. Given the 6-h interval (00, 06, 12, 18Z) per day, each daily CFS ensemble contained four members. Since the full 9-month runs of the CFSv2 reforecast only provides data every 5 days, we could only examine six lead times each month, designated as day zero through day 25 (d-0, d-5, d-10, d-15, d-20, and d-25¹). Each lead time was computed from the 28-year records with the initialization day designated as d-0. These same dates were also used in the observational and reanalysis data, denoted as Z_{OBS} and P_{OBS} . While we were aware of the available 45-day daily re-forecasts of CFSv2 over the period of 1999–2010, our goal of obtaining the empirical relationship between the upper-level circulations and regional precipitation was better served by analyzing a longer time period of data. Additionally, we focused our prediction estimates around a 30-day window and categorized the results by month.

3 Methodology and results

3.1 Identifying wavenumber linkages with precipitation

Adopting the climate divisions of the continental United States (CONUS) defined by the National Climate Assessment (NCA), we divided the CONUS into six regions; these are outlined in Fig. 1 and labeled R1–R6. Based upon the results of Schubert et al. (2011) and Wang et al. (2013a) which identified the upper tropospheric short-wave train, we used the 200-hPa Z to perform a regression analysis with precipitation averaged from these six regions. To

¹ For example, forecasts initiated on 6, 11, 16, 21, 26, and 31 May were used as d-25, d-20, d-15, d-10, d-5, and d-0 lead times for June; 5, 10, 15, 20, 25, and 30 June (July) were used as d-25, d-20, d-15, d-10, d-5, and d-0 lead times for July (August). Lead time nomenclature is similar to that used in Zuo et al. (2013).

Fig. 2 Flow chart detailing procedure used to create and compare the spatial correlations of regression between Z200 and precipitation for CFSv2 and observation datasets. Procedure produces a spatial correlation of regression score for each grid point across the $2.5^\circ \times 2.5^\circ$ grid CONUS grid. See text for details

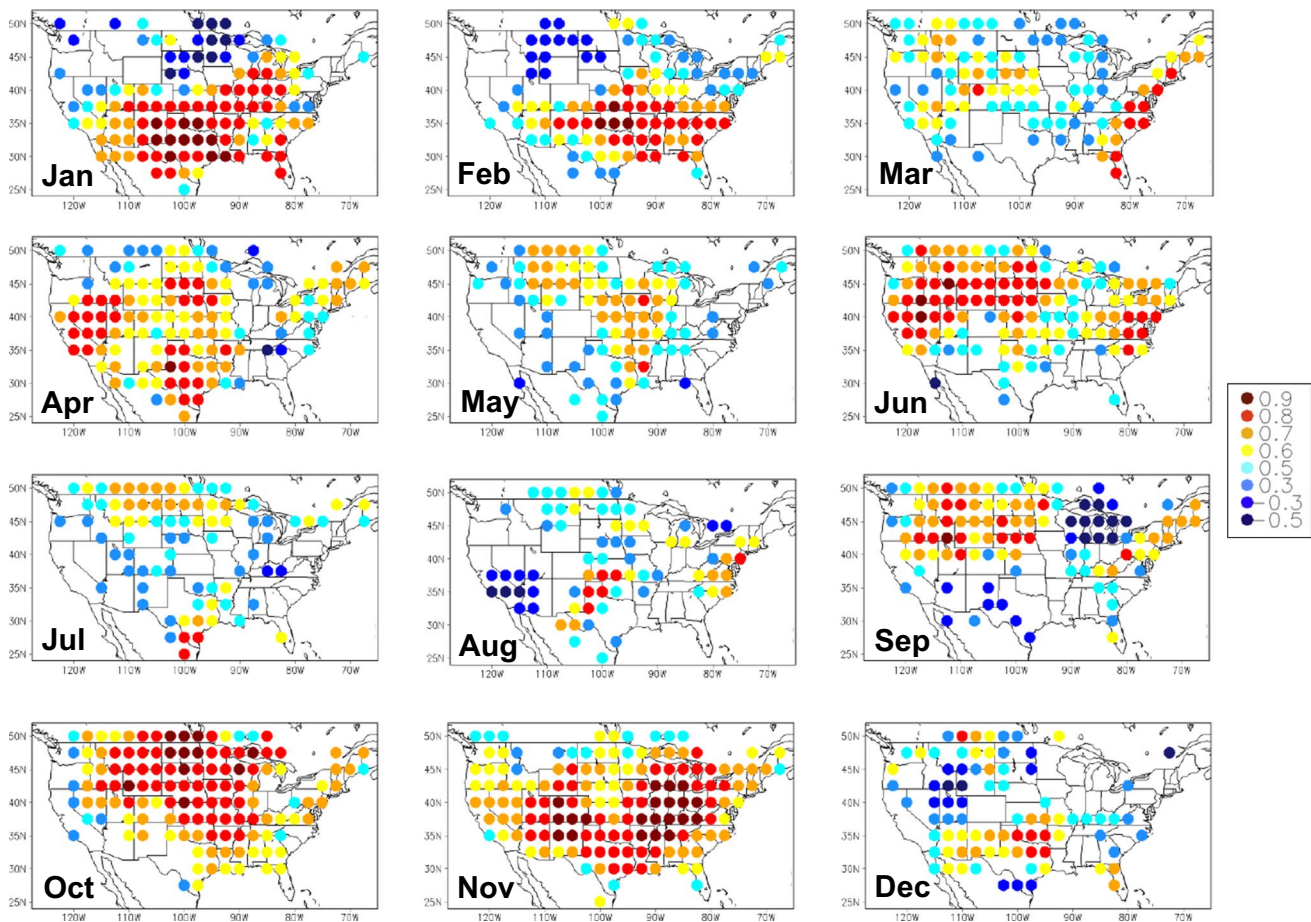
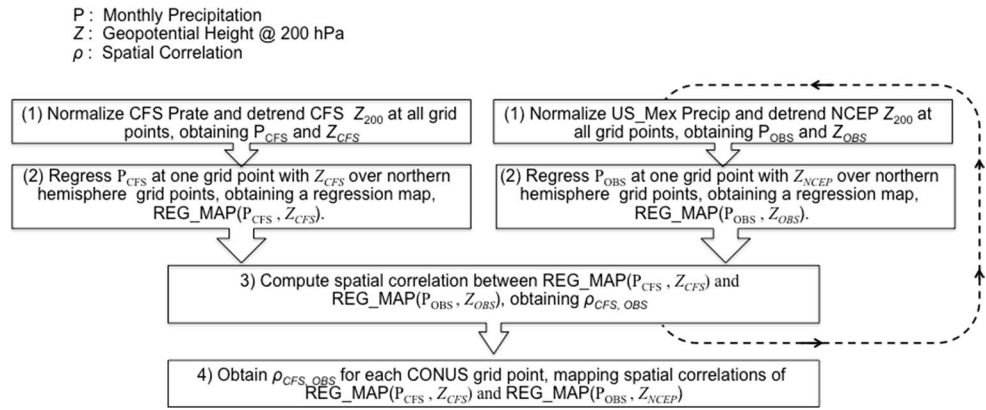


Fig. 3 Map of monthly spatial correlation of regression scores using d-0 lead times for wave-5 Z200 and precipitation relationships (other wavelengths not shown). Figure is the result of the scoring procedure presented in Fig. 2 and discussed in the text

begin with, we used d-0 to create a 30-day “baseline” for the evaluation of regression between P_{CFS}/Z_{CFS} and P_{OBS}/Z_{OBS} . Later, we used this baseline to evaluate the d-5, d-10, d-15, d-20, and d-25 forecasts, each comprising an average of 30 days starting from the initial day.

The identification procedure of an effective zonal wavenumber in the upper-level circulation follows that

of Wang et al. (2013a), but utilizes 200-hPa Z instead of the 250-hPa streamfunction; this procedure is illustrated in the flow chart of Fig. 2, modified from Fig. 3 of Wang et al. (2013a). The procedure may seem complicated, but is essentially a series of temporal regression and spatial correlation analyses applied between the P and Z fields and, in this case, extended to both the observational and

Table 1 (a) List of 19 candidate combinations of region, month, and wavenumber. Consists of 10 unique region and month combinations tested by P_{proxy} equation. Where multiple wavenumbers met the criteria set forth in Fig. 5, we performed the proxy analysis using the wavenumber with the highest absolute maxima and minima values within the regression pattern. (b) same as for (a), only listing the 9 successful candidate combinations of P_{proxy} shown in Fig. 5

Region	Month	Wavenumbers
(a)		
1	Jun	4,5,6
2	Jun	4,5,6
2	Nov	4
3	Jan	4,5
3	Feb	4,5
4	Jan	4
4	Oct	5
4	Nov	3,4,5
5	Nov	5
6	Nov	3,4
(b)		
1	Jun	4
2	Nov	4
3	Jan	5
3	Feb	5
4	Jan	4
4	Oct	5
4	Nov	5
5	Nov	5
6	Nov	4

CFSv2 reforecast data. The essentials comprise the isolation of zonal wavenumbers 1–6 from the 200-hPa Z_{CFS} and Z_{OBS} using Fourier series transform. Both P_{CFS} and P_{OBS} at each individual grid point were normalized based upon their standard deviation; this was to eliminate climatological biases in CFSv2, since quantitative precipitation forecast was not our focus here. A series of reforecast regression maps were created between P_{CFS} and corresponding Z_{CFS} over the Northern Hemisphere. Corresponding observed regressions between P_{OBS} and Z_{OBS} were created as well. Next, for each grid point within the CONUS domain, a spatial correlation between the reforecast regression map and observed regression map was computed; this process was repeated for each month based upon the d-0 lead time. The purpose of the analysis was to identify the combinations of region, wavenumber, and month in which the temporal regression pattern of $P_{\text{CFS}}/Z_{\text{CFS}}$ best matched those of $P_{\text{OBS}}/Z_{\text{OBS}}$. The idea is that where and when these patterns were most similar, it would be more likely that regional precipitation can be successfully linked to the 200-hPa Z field. The analysis

outlined by the flow chart of Fig. 2 was then applied to all wavenumbers (1–6) in all months.

In order to gauge the degree of similarity between the regression patterns, and also to ensure a normal distribution, we transformed the correlation values to z scores using Fisher's z transformation. We performed next an upper-tailed z-test with $\alpha = 0.10$ to identify a set of combinations in which the null hypothesis that no positive correlation pattern between the spatial regression features existed could be rejected. Of the 432 possible region, wavenumber, and month combinations, 25 were found to be greater than the critical z value of 1.282. Subsequently, we compared the magnitude of the linkages between the $P_{\text{CFS}}/Z_{\text{CFS}}$ and $P_{\text{OBS}}/Z_{\text{OBS}}$ regression patterns by performing a two-tailed F-test in which the null hypothesis stated that the variance of the two regression patterns were the same. Only combinations in which the F-test indicated insufficient evidence to reject the null hypothesis at the $\alpha = 0.05$ significance level ($F > 1.9$) were retained. Applying the F-test led to a reduction of top z-score combinations from 25 to 19. These objectively obtained combinations, as listed in Table 1a, represented when and where the CSSv2 hindcast best resolved the linkages between a given wavenumber and the corresponding precipitation anomalies in a given region.

3.2 Results of precipitation response to short-wave circulation

To illustrate the outcome of the procedure presented in the flow chart, Fig. 3 shows the spatial correlations of wave-5 at each grid point across the CONUS. One can visually identify clusters of high spatial correlation indicating the "scores" of temporal regression between P and Z from each month (hereafter referred to as scores). Of particular note are clusters of high scores across the southern U.S. in January and a spatial extent of high scores across vast stretches of the CONUS in June, October and November. Clusters of negative scores indicate locations of an inverse relationship between CFSv2 and observation correlations, indicating poor forecast skill or a lack of predictability within the short-wave circulation framework. Nevertheless, the presence of clustered positive scores shows that, at certain wavenumbers, CFSv2 can capture the linkages between the upper-level short-wave circulations and the regional precipitation responses at certain time/location combinations.

The dependence of model performance on month and location is likely caused by the unique jet stream position and terrain features that affect the stationary short-waves at different times of the year, as was discussed in Wang et al. (2013a). For instance, the high scores in June over the

Midwestern U.S. reflect a key feature of the short-wave/precipitation connection (Schubert et al. 2011) and, based on Fig. 3, this feature is reasonably resolved by CFSv2. A potential predictability is also revealed from the relationship between wave-5 pattern and regional precipitation in January, October, and November. The months of February, April, and September show isolated regions of moderate predictability. The months of December, March, May, July, and August show the poorest scores in terms of the wave-5 linkage to precipitation. However, this outcome cannot be interpreted as a result of poor model performance, as December and March have previously been identified as having the weakest correlations of precipitation with the short-wave pattern (Wang et al. 2013a). Additionally, the CGT in July often operates on even shorter wavelengths (wavenumber 6–8) (Ding and Wang 2005). Some poor performance may also be tied to differences in the initial conditions of the 200-hPa Z in the CFSv2 model and NCEP1 reanalysis: At the scale of the northern hemisphere mid-latitude region such differences would be minimal. More pronounced errors in the initial conditions exist between modeled CFSv2 precipitation rate and the observed CPC unified precipitation product. While we acknowledge that differences in initial conditions could have some influence, we do not quantify them here. Such differences would exist when comparing any model to an observational dataset and is not part of the objectives of this analysis.

Equipped with both the spatial and variance comparisons, we present all 432 possible region, wavenumber, and month combinations with the Taylor diagrams in Fig. 4. Spatial correlation of regression scores, like those in Fig. 3, are shown along the radial axis. Ratio of Variance (RVAR) values, equivalent to the F-statistic, are displayed along the x and y axes. Ideal combinations occur where both metrics are equal to 1, or where the red radial line touches the x-axis. The objectively identified 19 z-score combinations are highlighted by their months for each region.

It is important to note that of the 19 combinations, all but two fall within our targeted short-wave regime (wavenumbers 4–6); this is an encouraging finding as such short-wave circulation patterns exhibit considerable influence on downstream precipitation anomalies on the monthly time-scale. The aforementioned results are supportive of the next step, that is, to predict monthly precipitation anomalies based on the circulation-based proxy rather than using the CFSv2 precipitation output directly.

3.3 Development of precipitation proxy

In order to provide an assessment of potential predictability, we used the 200-hPa Z as the sole predictor independent of the precipitation output. Using the selected months

in Fig. 4, we developed a precipitation proxy equation for the selected regions. Figure 5 displays eight scenarios of the regression patterns between regional precipitation (indicated on top of each panel) and filtered 200-hPa Z waves (as noted in the upper right of each panel). From the regression maps, we chose two sets of Z anomaly cells occurring in tandem directly upstream or within one half wavelength downstream from the region of interest. These maxima and minima locations are indicated by the black boxes on the regression maps of Fig. 5.

While 19 combinations of region, wavenumber, and month were identified in Sect. 3.1 to construct the precipitation proxy, it can be seen from Table 1a that multiple wavenumbers often met the criteria for a given region and month. In such cases, we performed the proxy analysis using the wavenumber with the highest absolute maxima and minima values within the regression pattern; this reduced our 19 candidate combinations to 10 unique pairs of target regions and month. Next, we produced the 200-hPa Z anomalies during each year of 1982–2009. The Z anomaly values were extracted from each of the short-wave cells outlined by the black boxes in Fig. 5 (i.e., $L_{1,2,3,4}$) and used as predictors for the 30-day mean of observed precipitation. The result led to multiple linear regression coefficients ($C_{1,2,3,4}$) for each cell location ($L_{1,2,3,4}$). The combination of the coefficients and 200-hPa Z anomaly values, along with the intercept (correction value), derives the 30-day precipitation proxy (P_{proxy}) in the following equation:

$$P_{\text{proxy}} = L_1 * C_1 + L_2 * C_2 + L_3 * C_3 + L_4 * C_4 + \text{intercept} \quad (1)$$

Using Eq. (1), P_{proxy} was produced for each of the 10 targeted pairs using all six lead times (d-0, d-5, d-10, d-15, d-20, and d-25). To evaluate this precipitation proxy against the direct model output of precipitation, we created equivalent time series of regional precipitation estimates directly from CFSv2 (P_{CFS}) averaged from the same 10 targeted region and months (Table 1a) at all six lead times. Temporal correlation scores were then computed between P_{proxy} and P_{CFS} as a measure to determine model performance.

3.4 Evaluation of the forecast of precipitation proxy

The results of the comparison between P_{proxy} and P_{CFS} are presented in the line graphs of Fig. 5 next to each map. Temporal correlation scores are shown on the y-axis while lead times (d-0 through d-25) are shown on the x-axis. Red lines show correlation scores for P_{proxy} with blue lines showing scores for the direct P_{CFS} forecasts. Correlation scores are smoothed using 3-point averages, except at d-0 and d-25 which are smoothed only by two points. Of the 10 unique region and month combinations, 9 combinations (listed in Table 1b) exhibit significantly and persistently

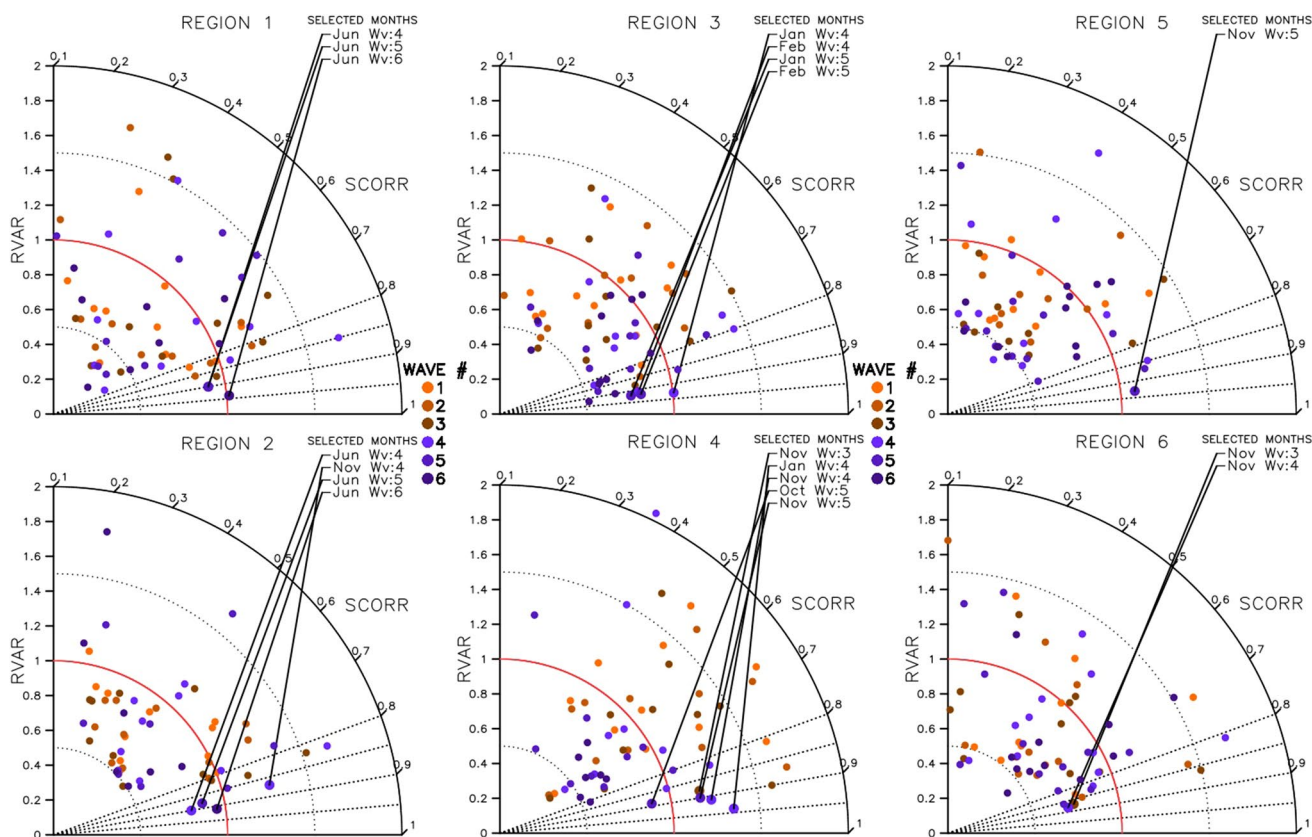


Fig. 4 d-0 Taylor diagram plots for region R1–R6. X–Y axis shows RVAR values while radial axis shows spatial correlation score. All month and wavenumber (1–6) combinations are shown for each

region. Selected months are identified through the combination of an upper-tailed Z test and an F-test for difference in variance as outlined in Sect. 3.1 of the text

higher correlations in P_{proxy} than in P_{CFS} . The combinations shown in Fig. 5 and listed in Table 1b are those with correlation scores of P_{proxy} exceeding P_{CFS} at three or more of the six lead times. Within the admittedly small sample of combinations, over 80 % show that the developed P_{proxy} outperformed P_{CFS} .

These results are encouraging as the methodology presented in Sect. 3.1 can easily be adjusted to include either broader or narrower spatial/temporal scales for further improvement. Obviously, the prediction of P_{proxy} relies upon natural circumstance, for if no anomalous short-wave circulations develop in a given month, then there would be no useful skill gained by the P_{proxy} method. Thus, the operational potential of this approach exists only as a forecast of opportunity, relying on the formation and stagnation of these type of shortwave features. The regional average of rainfall (P) as was used in this study also does not depict any spatial distribution of the P anomalies. Nonetheless, our analysis did identify which months and regions are most likely to benefit from successful predictions of upper-level circulation anomalies by CFSv2. The results of this method provide a realization for the implications

learnt from previous research such as those of Schubert et al. (2011), Wang et al. (2013a, 2014) in that the linkage between standing Rossby short-waves and local precipitation can provide predictability at long lead times.

4 Concluding remarks

We explored the subseasonal predictive capabilities of CFSv2 towards resolving the relationship between short-wave circulation patterns and regional precipitation anomalies as previously documented in the literature. By exploring the optimal combinations amongst zonal wavenumber, region, and month, we developed a precipitation proxy (as a function of the short-wave circulation) and evaluated it against the forecast of direct precipitation model output. Results were variable both spatially and temporally, with the highest forecast skill/score coinciding with the stronger signals in the short-wave circulations. The forecast performances were associated with the variability in jet locations and stationary wave patterns among individual months. Depending on the region and month of the year, it can be

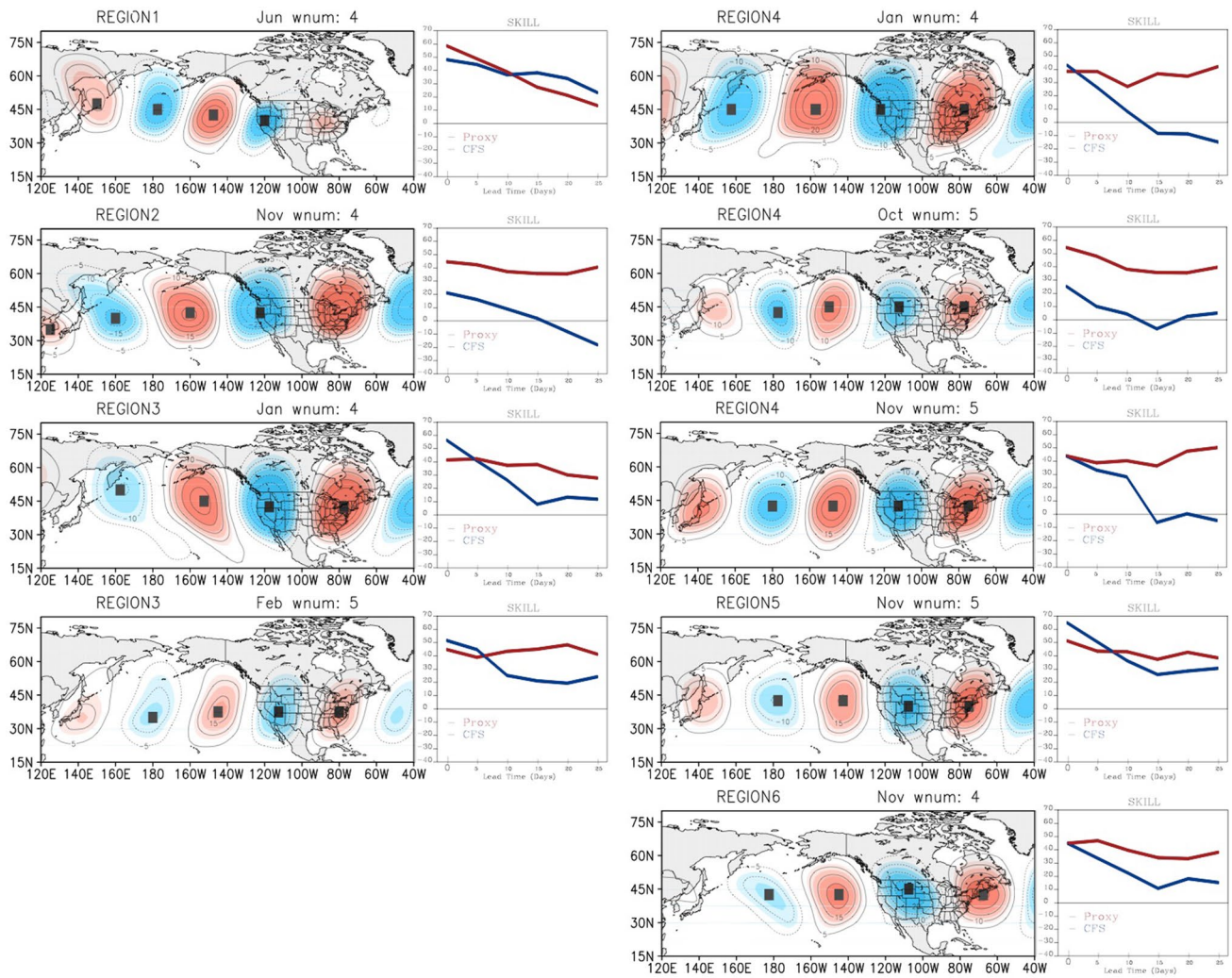


Fig. 5 Nine combinations of the proxy equation determined have better temporal correlations between predicted and observed precipitation. The *left hand sides* are maps of the 1982–2009 regression patterns for wavelength, month, and region combinations as indicated above each figure panel. Filled *black boxes* outline the index locations

($L_{1,2,3,4}$) used in Eq. (1). The *right hand sides* show both the Pproxy and CFSv2 temporal correlation scores. *Lines* were smoothed using 3-point averages, except at d-0 and d-25, which are smoothed only by two points

concluded that, over CONUS, there is a potential for sub-seasonal (week 3–4) precipitation forecasts if one considers the short-wave circulation features as the proxy of regional precipitation anomalies.

Why would a simple statistical approach outperform the model precipitation output so much? It could be argued that the parameters used in the present method are forced by the choices of using a narrow region and/or a narrow period such that it would be sensitive to the reanalysis product or CFSv2. However, this is precisely the point of our focus on the usage of short-wave circulations, since such circulation regimes produce narrow, region-specific impacts on precipitation variations. The fact that the proposed method appears to obtain generally higher skill scores than the

direct model output of precipitation (in certain regions/months) speaks to the value and feasibility in combining a dynamical prediction (CFSv2 Z field) with a statistical one (proxy for precipitation). Earlier research has also applied a similar hybrid approach in predicting winter temperature inversions in narrow mountain valleys (Gillies et al. 2010) and island diurnal afternoon thunderstorms (Wang et al. 2013b) using CFS model’s large-scale circulation pattern.

The methods of this study can be expanded globally to any mid-latitude region. Likewise, the focus region can also be narrowed to include any area known to be heavily influenced by the seasonal or subseasonal fluctuations in the jet position. Further exploration is needed to migrate this P_{proxy} method from being potentially useful

to operationally feasible. For future work, we propose the inclusion of the correlation scores from the various combinations (of region, month and wavenumber) as a “skill mask” to highlight where and when the subseasonal predictions from CFSv2 (or any multi-model ensemble product) can be given higher weight elsewhere. A similar procedure, looking at short-wave pattern influences on surface temperature anomalies, will compliment this study in the production of a similar temperature proxy.

Acknowledgments The authors thank two anonymous reviewers whose thorough review and comments greatly improved this paper. Conversations with Oi-Yu (JoJo) Chung regarding statistical methodologies were much appreciated. This research was partially supported by DOE DE-FOA-0001531 and SERDP 17-RCSEED01-002.

References

- Ambrizzi T, Hoskins B, Hsu HH (1995) Rossby wave propagation and teleconnection patterns in the austral winter. *J Atmos Sci* 52(21):3661–3672
- Becker EJ, Van Den Dool H, Peña M (2013) Short-term climate extremes: prediction skill and predictability. *J Clim* 26(2):512–531. doi:10.1175/JCLI-D-12-00177.1
- Branstator G (2002) Circumglobal teleconnections, the jet stream waveguide, and the North Atlantic Oscillation. *J Clim* 15(14):1893–1910
- Chen M, Xie P, et al (2008) CPC Unified Gauge-based Analysis of Global Daily Precipitation. In: Western Pacific geophysics meeting, Cairns, 29 July–1 August, 2008
- Ding Q, Wang B (2005) Circumglobal teleconnection in the northern hemisphere summer. *J Clim* 18(17):3483–3505
- Ding Q, Wang B, Wallace JM, Branstator G (2011) Tropical–extratropical teleconnections in boreal summer: observed interannual variability. *J Clim* 24(7):1878–1896
- Gillies RR, Wang SY, Yoon JH, Weaver S (2010) CFS prediction of winter persistent inversions in the intermountain region. *Weather Forecast* 25(4):1211–1218
- Hoskins BJ, Ambrizzi T (1993) Rossby wave propagation on a realistic longitudinally varying flow. *J Atmos Sci* 50:1661–1671
- Kalnay et al (1996) The NCEP/NCAR 40-year reanalysis project. *Bull Am Meteorol Soc* 77:437–470
- Saha S et al (2014) The NCEP Climate Forecast System version 2. *J Clim* 27:2185–2208. doi:10.1175/JCLI-D-12-00823.1
- Schubert S, Wang H, Suarez M (2011) Warm season subseasonal variability and climate extremes in the Northern Hemisphere: the role of stationary Rossby waves. *J Clim* 24(18):4773–4792
- Screen JA, Simmonds I (2014) Amplified mid-latitude planetary waves favour particular regional weather extremes. *Nat Clim Change* 4(8):704–709
- Sooraj KP, Annamalai H, Kumar A, Wang H (2012) A comprehensive assessment of CFS seasonal forecasts over the tropics*. *Weather Forecast* 27(1):3–27. doi:10.1175/WAF-D-11-00014.1
- Wang SY, Hipps LE, Gillies RR, Jiang X, Moller AL (2010) Circumglobal teleconnection and early summer rainfall in the US intermountain west. *Theor Appl Climatol* 102(3–4):245–252
- Wang S-Y, Davies RE, Gillies RR (2013a) Identification of extreme precipitation threat across midlatitude regions based on short-wave circulations. *J Geophys Res Atmos* 118:11059–11074
- Wang S-Y, Chia H-H, Gillies RR, Jiang X (2013b) Quasi-biweekly mode and its modulation on the diurnal rainfall in Taiwan forecasted by the CFS. *Weather Forecast* 28:981–993
- Wang H, Schubert S, Koster R, Ham Y-G, Suarez M (2014) On the role of SST forcing in the 2011 and 2012 extreme U.S. heat and drought: a study in contrasts. *J Hydrometeorol* 15:1255–1273
- Yuan X, Wood EF, Luo L, Pan M (2011) A first look at Climate Forecast System version 2 (CFSv2) for hydrological seasonal prediction. *Geophys Res Lett* 38:L13402. doi:10.1029/2011GL047792
- Zuo Z, Yang S, Hu Z-Z, Zhang R, Wang W, Huang B, Wang F (2013) Predictable patterns and predictive skills of monsoon precipitation in Northern Hemisphere summer in NCEP CFSv2 reforecasts. *Clim Dyn* 40:3071–3088